

Article

Anticancer Activity and Mode of Action of Cu(II), Zn(II), and Mn(II) Complexes with 5-Chloro-2-*N*-(2-quinolylmethylene)aminophenol

Shuangshuang Gai, Liqin He, Mingxian He, Xuwei Zhong, Caiyun Jiang, Yiming Qin * and Ming Jiang * 

Key Laboratory for Zhuang and Yao Pharmaceutical Quality Biology, School of Food and Biochemical Engineering, Guangxi Science & Technology Normal University, Laibin 546199, China; gaishuangshuang@gxstnu.edu.cn (S.G.); 13397802652@163.com (L.H.); hemingxian@gxstnu.edu.cn (M.H.); zhongxuwei@gxstnu.edu.cn (X.Z.); jiangcaiyun@gxstnu.edu.cn (C.J.)

* Correspondence: qym68@163.com (Y.Q.); jiangbiochem@163.com (M.J.); Tel.: +86-772-212-0958 (M.J.)

Abstract: Developing a new generation of anticancer metal-based drugs that can both kill tumor cells and inhibit cell migration is a promising strategy. Herein, we synthesized three Cu(II), Zn(II), and Mn(II) complexes derived from 5-chloro-2-*N*-(2-quinolylmethylene)aminophenol (C1–C3). Among these complexes, the Cu(II) complex (C1) showed significantly greater cytotoxicity toward lung cancer cell lines than cisplatin. C1 inhibited A549 cell metastasis and suppressed the growth of the A549 tumor in vivo. In addition, we confirmed the anticancer mechanism of C1 by triggering multiple mechanisms, including inducing mitochondrial apoptosis, acting on DNA, blocking cell cycle arrest, inducing cell senescence, and inducing DNA damage.

Keywords: anticancer; DNA; metal complexes; lung cancer



Citation: Gai, S.; He, L.; He, M.; Zhong, X.; Jiang, C.; Qin, Y.; Jiang, M. Anticancer Activity and Mode of Action of Cu(II), Zn(II), and Mn(II) Complexes with 5-Chloro-2-*N*-(2-quinolylmethylene)aminophenol. *Molecules* **2023**, *28*, 4876. <https://doi.org/10.3390/molecules28124876>

Academic Editor: Fabio Marchetti

Received: 9 May 2023

Revised: 8 June 2023

Accepted: 12 June 2023

Published: 20 June 2023



Copyright: © 2023 by the authors. Licensee MDPI, Basel, Switzerland. This article is an open access article distributed under the terms and conditions of the Creative Commons Attribution (CC BY) license (<https://creativecommons.org/licenses/by/4.0/>).

1. Introduction

Cisplatin is widely used to treat various solid tumors; it can induce cancer cell apoptosis by acting on DNA and results in cancer cell death [1,2]. However, the clinical application of cisplatin is limited because of the following factors: (1) easy-to-develop drug resistance [3,4]; (2) severe side effects on organs [1,5,6]; and (3) stimulating metastasis of cancer [7–9]. Accordingly, current anticancer metal-based drug research focuses on developing compounds with other metal centers, which may be a promising strategy.

Currently, to develop the next generation of metal drugs and realize effective anti-cancer treatment, Cu, Ru, Zn, Au, Mn, and other metal complexes have been widely synthesized for tumor therapy, which may exhibit different anticancer functions and specific patterns [10–14]. Among them, Cu, Zn, and Mn are essential trace elements in the human body, which are vital in maintaining human health and physiological activities [15–17]. Furthermore, Cu, Zn, and Mn complexes strongly inhibit cancer cell growth and have high selectivity [14,18,19].

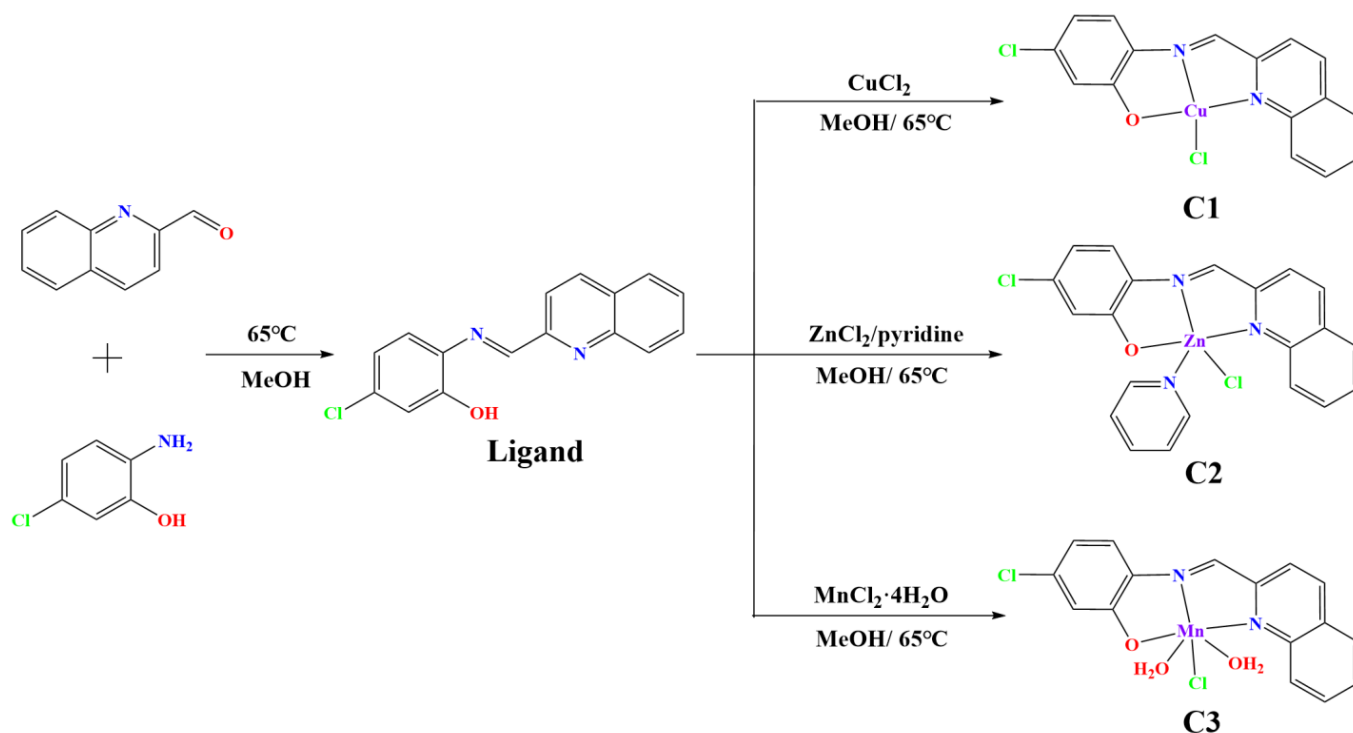
The Schiff base is a condensation product of primary amine and aldehyde (or ketone) compounds, in which the resulting azomethine nitrogen atoms have very important biological activities, including antitumor properties [20–23]. Aminophenol Schiff base ligands have recently gained extensive attention because they have good antitumor activity [24–27], and they possess strong coordination ability and diverse coordination modes owing to their oxygen and nitrogen atoms coordination sites [28,29]. Interestingly, several metal complexes have also been synthesized using aminophenol Schiff base ligands and have shown remarkable antitumor activity [24,28,30]. However, there still remain mysteries about their antitumor mechanism. Therefore, we proposed to design a novel non-Pt compound based on 5-chloro-2-*N*-(2-quinolylmethylene) aminophenol Schiff base ligand, which may be a promising approach to enhance selectivity.

Considering the above factors, we designed and synthesized a series of non-Pt (Cu^{II} , Zn^{II} , and Mn^{II}) complexes (C1, C2, and C3, respectively) derived from 5-chloro-2-*N*-(2-quinolylmethylene) aminophenol Schiff base ligand and assessed their anticancer activity. Among them, the Cu complex (C1) exhibited the highest anticancer activity. Subsequently, we investigated the antimetastasis ability of C1 and confirmed the mechanism of C1 multi-actions on lung cancer cells. Finally, we further evaluated the antitumor activity of C1 in mice bearing A549 tumor. Our results provide new insights to develop novel non-Pt complexes with potent antitumor and antimetastasis activities.

2. Results and Discussion

2.1. Synthesis and Characterization of Cu(II), Zn(II), and Mn(II) Complexes

The Schiff base ligand (L) was formed by reacting 2-quinolinecarboxaldehyde with 5-chloro-2-aminophenol in methanol. Subsequently, the corresponding Cu(II), Zn(II), and Mn(II) complexes were synthesized in situ (Scheme 1). Single crystals of Cu(II), Zn(II), and Mn(II) complexes were determined using X-ray crystallography and solved using Olex 2.0 software. The molecular structures of Cu(II), Zn(II), and Mn(II) complexes (C1–C3) are shown in Figure 1. The crystallographic data of these complexes are reported in Tables S1 and S2.



Scheme 1. Synthetic route for C1–C3.

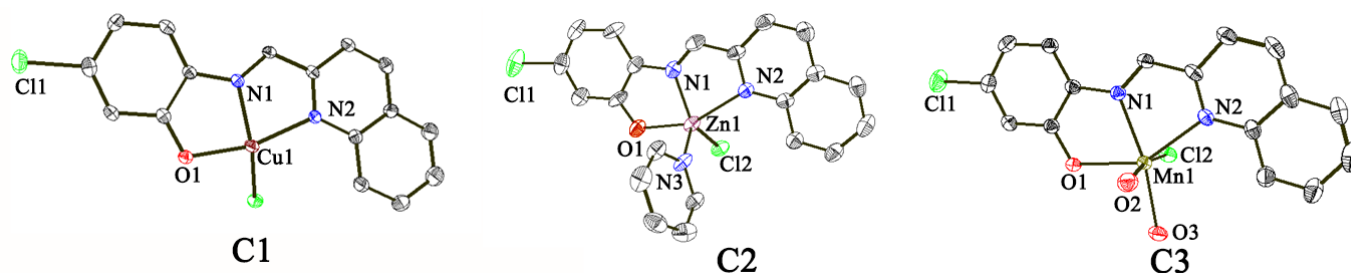


Figure 1. Crystal structures of Cu(II), Zn(II), and Mn(II) complexes (C1–C3).

C1 crystallizes in the monoclinic system with the space group $P2_1/c$. The coordination geometry of Cu^{2+} is square planar with one quinoline-N [Cu1–N2 = 2.076(3) Å], one imine-N [Cu1–N1 = 1.944(3) Å], one phenolate-O [Cu1–O1 = 1.959(3) Å] from ligand, and one Cl atom [Cu1–Cl1 = 2.2479(11) Å].

C2 crystallizes in the triclinic system with the P-1 space groups. The center Zn^{2+} adopts a square pyramidal distortion. Two N and one O atoms donated by the Schiff base ligand (N1, N2, and O1) and one Cl atom (Cl2) form a plane. The other N (N3) from pyridine is positioned at the vertex.

C3 crystallizes in the triclinic system with the space group P-1; the distorted octahedral coordination sphere around the Mn^{2+} is assembled from the N,N,O-tridentate ligand, two H_2O ligands, and one Cl^- ion.

The structures of L and C1–C3 were further characterized (Figures S1–S12). In the IR spectra of L, the peaks at 2315 and 1796 were attributed to the $\nu_{\text{C=N}}$ stretching bands; the peak at 3736 cm^{-1} corresponded to the stretching vibrations of phenolic $\nu_{\text{O-H}}$. When L formed complexes (C1–C3) with metal ions, the peak of $\nu_{\text{O-H}}$ disappeared and the peaks of C=N were shifted. The complexes were confirmed by comparing the IR spectra of C1–C3 and L. In addition, the $^1\text{H-NMR}$ and $^{13}\text{C-NMR}$ spectra of L (Figure S1) and C2 were measured and were found to be consistent with the expected structures.

2.2. The Solubility and Stability of Cu(II), Zn(II), and Mn(II) Complexes in Saline

In order to carry out the following biological activity assays, we tested the solubility of the metal complexes in saline (0.9% sodium chloride solution). The solubility of C1, C2, and C3 was ≥ 1.9 , 1.3, and 0.8 mg/mL, respectively. These results indicated C1–C3 had good solubility in saline. Then, we further evaluated the stability of C1–C3 in saline by UV-vis spectroscopy. As shown in Figure S13, there were no significant changes of absorbance spectra for 48 h, indicating that C1–C3 were stable in saline for 48 h. Therefore, C1–C3 were dissolved in saline for subsequent cell assays.

2.3. The Cytotoxicity of Cu(II), Zn(II), and Mn(II) Complexes In Vitro

The cytotoxicity of C1–C3 was determined using an MTT (3-(4,5-dimethylthiazol-2-yl)-2,5-diphenyltetrazolium bromide) assay on various cancer cells. As shown in Table 1, the IC_{50} values of the Schiff base ligand were significantly higher than those of the metal complexes. The Cu complex (C1) exerted the highest cytotoxic potency compared with the Zn(II) and Mn(II) complexes in A549 cells, with IC_{50} values of 3.93 μM , while IC_{50} values of C2 and C3 were 18.26 and 33.61 μM , respectively. In addition, C1 had the most potent activity against cisplatin-resistant lung cancer (A549cisR) cells. Notably, compared to cisplatin, Cu complexes not only had superior anticancer activity, but also exhibited better selectivity. Therefore, C1 was selected to carry out the following studies.

Table 1. IC_{50} (μM) values of Cu(II), Zn(II), and Mn(II) complexes against various cell lines.

| Compound | A549 | MCF-7 | Hela | A549cisR | WI-38 | SI ^a |
|-----------|--------------|--------------|--------------|--------------|--------------|-----------------|
| L | >40 | >40 | >40 | >40 | >40 | - |
| C1 | 3.93 ± 0.28 | 5.30 ± 0.35 | 6.31 ± 0.32 | 6.79 ± 0.38 | 10.22 ± 0.43 | 2.60 |
| C2 | 18.26 ± 0.52 | 23.61 ± 0.98 | 22.75 ± 0.80 | 29.33 ± 0.85 | 33.96 ± 1.06 | 1.86 |
| C3 | 33.61 ± 0.98 | >40 | >40 | >40 | >40 | - |
| Cisplatin | 12.54 ± 0.45 | 14.53 ± 0.48 | 15.33 ± 0.51 | >40 | 9.61 ± 0.58 | 0.77 |

^a Selectivity index (SI) is determined as IC_{50} (WI-38)/ IC_{50} (A549).

2.4. Inhibition of C1 on Migration and Invasion Activities

Cell migration is crucial to cancer development and metastasis [31,32]; metastasis is a major cause of many cancer-related deaths [33,34]. The migration is very usually assessed by the application of the wound-healing assay, which involves the creation of an artificial gap in a cancer cell monolayer, followed by observation of the area covered with migrating cells [35]. Therefore, the inhibiting effect of C1 on cancer cell migration was evaluated using

a wound-healing assay. Figure 2A shows that the significant migration of A549 cells to the blank area in the control group compared with that in the C1 group, indicating that C1 strongly inhibited the migration ability of A549 cells. In addition, the effect of C1 on A549 cell invasion was investigated using a transwell assay. The number of cells that invaded across the inserts was significantly lower in the C1-treated group than in the untreated group (Figure 2B), indicating that C1 could inhibit the invasion abilities of A549 cells.

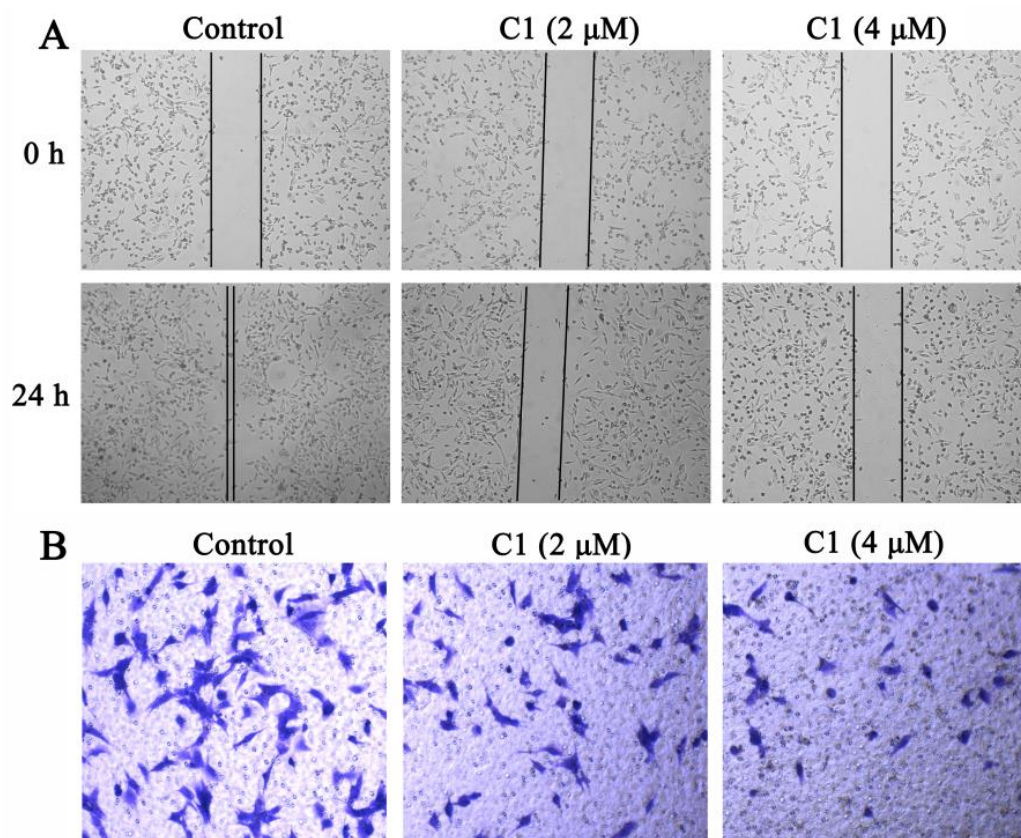


Figure 2. (A) The anti-migratory effect of C1 on A549 cells by wound-healing assay. (B) A549 cells' invasion ability with C1 treatment for 24 h in transwell assays.

2.5. Mechanism of Action of C1

2.5.1. Inducing Mitochondrial-Mediated Apoptosis

Mitochondria play a key role in death signals through intrinsic and extrinsic apoptosis [36,37]. Therefore, after exposure to C1, A549 cells were stained with a JC-1 probe to evaluate the mitochondrial membrane potential ($\Delta\Psi_m$) using flow cytometry. The results from Figure 3A showed that the $\Delta\Psi_m$ of A549 cells was reduced by 17.3% and 23.7% when treated with C1 at concentrations of 4 and 8 μM, respectively, strongly indicating that C1 altered $\Delta\Psi_m$ and induced mitochondrial dysfunction.

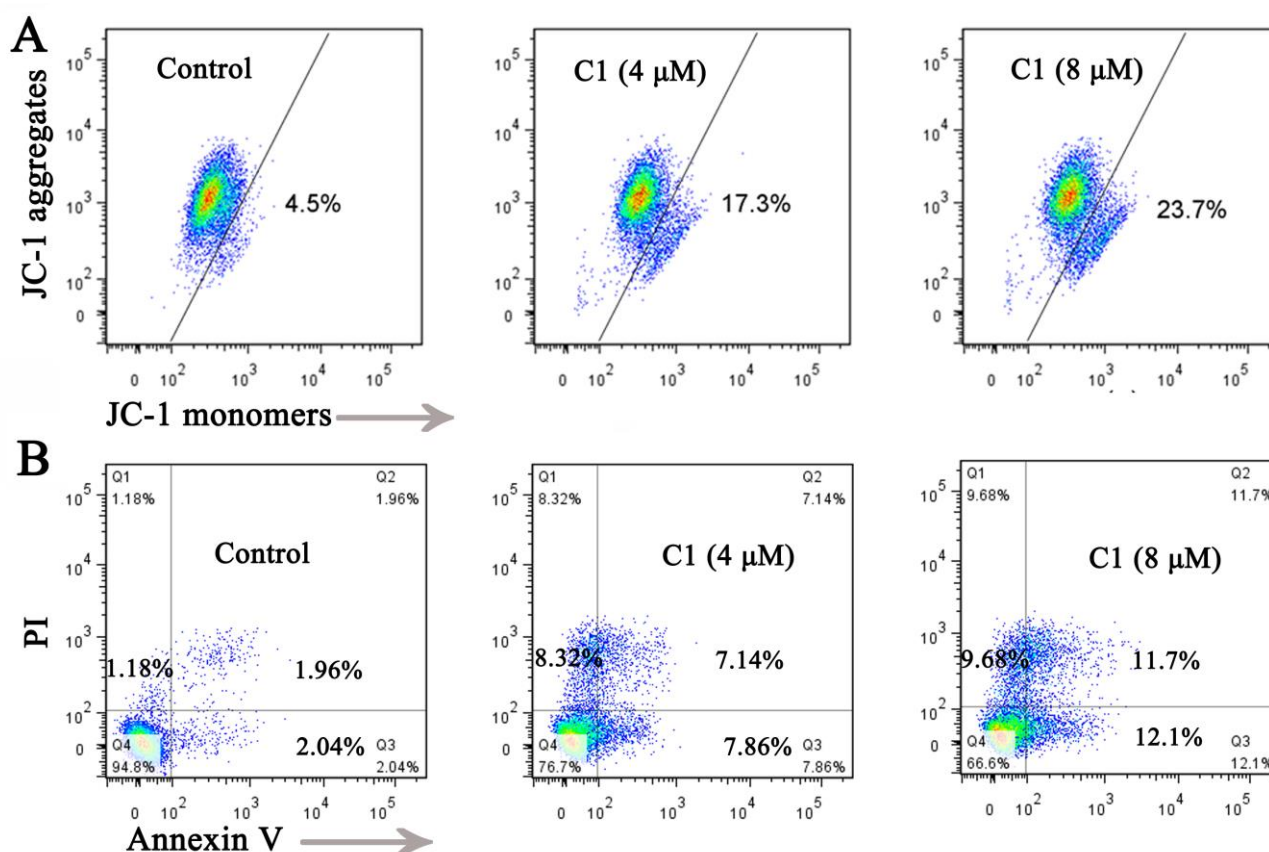


Figure 3. (A) JC-1 staining of C1-treated A549 cells detected using flow cytometry. (B) The effect of C1 on A549 cells apoptosis after treatment with C1 for 24 h.

Then, the effect of C1 on A549 cells apoptosis was stained with Annexin V/PI and analyzed using flow cytometry. Figure 3B indicates that when A549 cells were treated with C1, the population of apoptotic cells considerably increased (15.0% and 23.8% for 4 and 8 μM , respectively) compared to the control group (4.0%), suggesting that C1 induced apoptosis in A549 cells.

2.5.2. DNA Binding

Competitive studies with ethidium bromide (EB) have been widely used in fluorescence-quenching assays to evaluate the interaction between DNA and small molecules [38]. Therefore, to further explore the binding property of C1 and DNA, fluorescence quenching was carried out to explore the interaction mode. As shown in Figure 4A, the EB-DNA solution emits strong fluorescence at 550–750 nm, and the maximum fluorescence appears at 601 nm. As the C1 content increased, a decrease in the emission intensity was observed, indicating that C1 exhibited better competitive ability than EB and displaced EB from the hydrophobic pockets of DNA. These results verified that C1 binds to DNA in an intercalative binding mode.

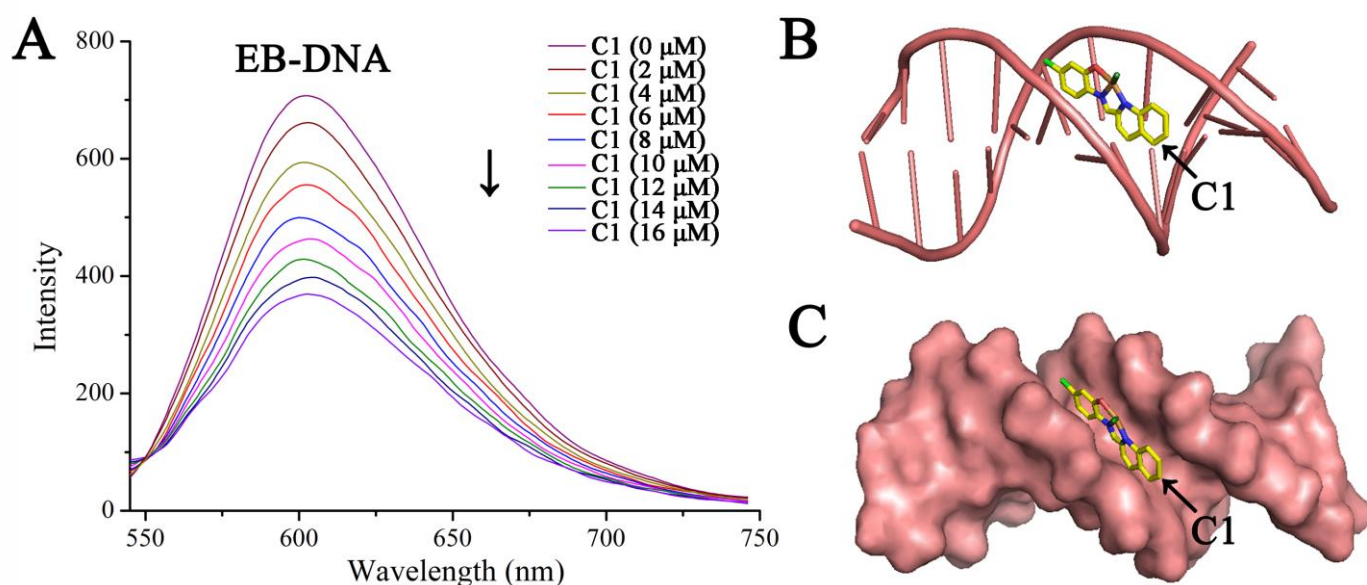


Figure 4. (A) The emission spectra of EB-DNA with successive addition of C1. (B,C) Docked pose of Cu complex and DNA.

Next, docking studies were conducted to investigate the interaction between C1 and DNA. According to our docking calculations, the docked binding energy value was -7.63 kcal/mol. As shown in Figure 4B,C, the Cu complex fit well into the curved profile in a minor groove of DNA (PDB ID: 1D64), and formed hydrogen bonds with surrounding bases. As a result, C1 can be stably intercalated in the double helix DNA strand in a similar mode to similar aminophenol Schiff base derivatives [39].

2.5.3. Arresting Cell Cycle

The influence of metal compounds on cell cycle arrest contributes to their anticancer activity [40]. To determine the effect of C1 on the cell cycle, the distribution of the cell cycle of C1-treated A549 cells was detected using flow cytometry. As shown in Figure 5, after treatment with 4 and 8 μM C1 for 48 h, the percentage of cells in the G1/G0 phase increased to 48.85% and 54.45%, respectively. This result indicates that C1 can block the A549 cell cycle in the G1/G0 phase.

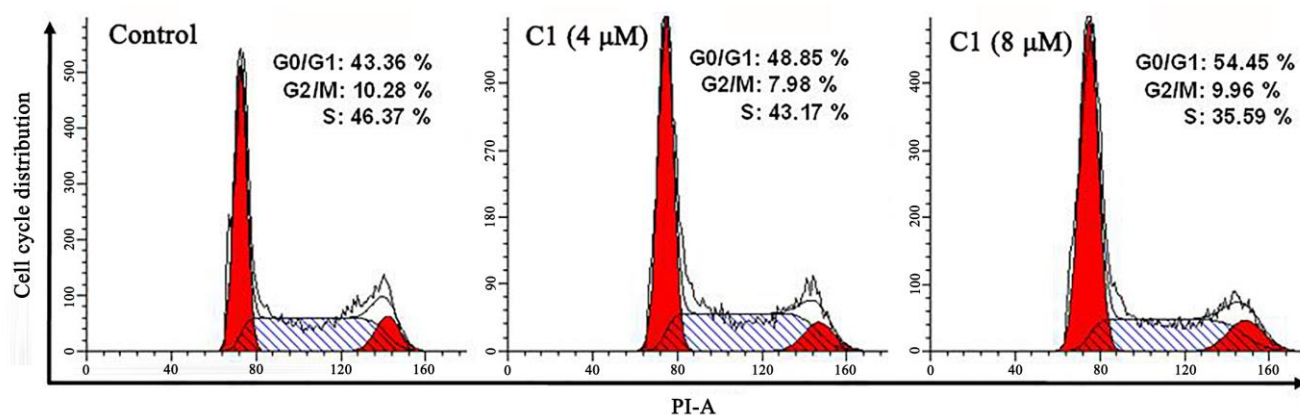


Figure 5. The effect of C1 on the cell cycle in A549 cells after treatment for 48 h, analyzed using flow cytometry.

2.5.4. Inducing A549 Cell Senescence

Senescence is a permanent cellular stage involving cell cycle arrest, which is a potential strategy against cancer [41]. We measured the impact of C1 on cell senescence in A549 cells using a β -galactosidase staining assay. The senescent cells were dyed blue by β -galactosidase. As shown in Figure 6, the number of blue-stained cells was significantly higher in the C1 group compared to that observed in the control group, and the C1-treated cells were accompanied by noticeable morphological changes. These results suggested that C1 can induce A549 cell senescence.

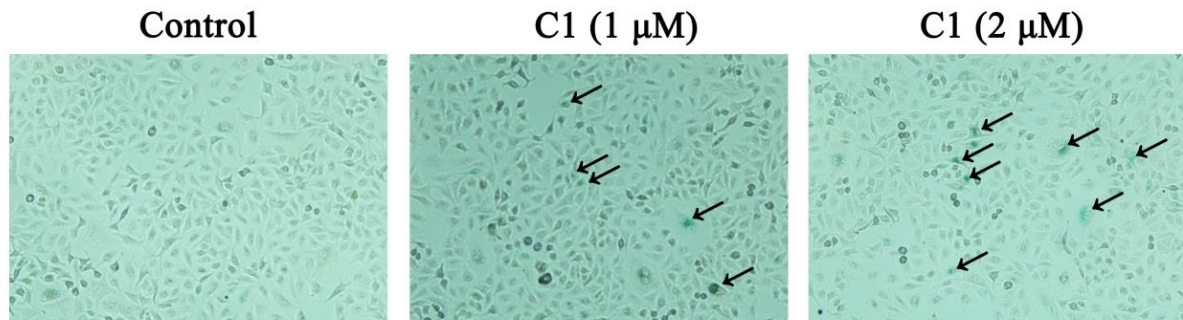


Figure 6. Cell senescence after treatment with C1, studied using a β -galactosidase staining assay (senescent cells marked by black arrows).

2.5.5. Inducing DNA Damage

A change in the mitochondrial membrane potential results in mitochondrial dysfunction, which can induce reactive oxygen species (ROS) production [42]. Based on the above information, we detected the ROS level in A549 cells using flow cytometry. As shown in Figure 7A, the intracellular ROS was significantly increased after treating the cells with C1 compared to the control.

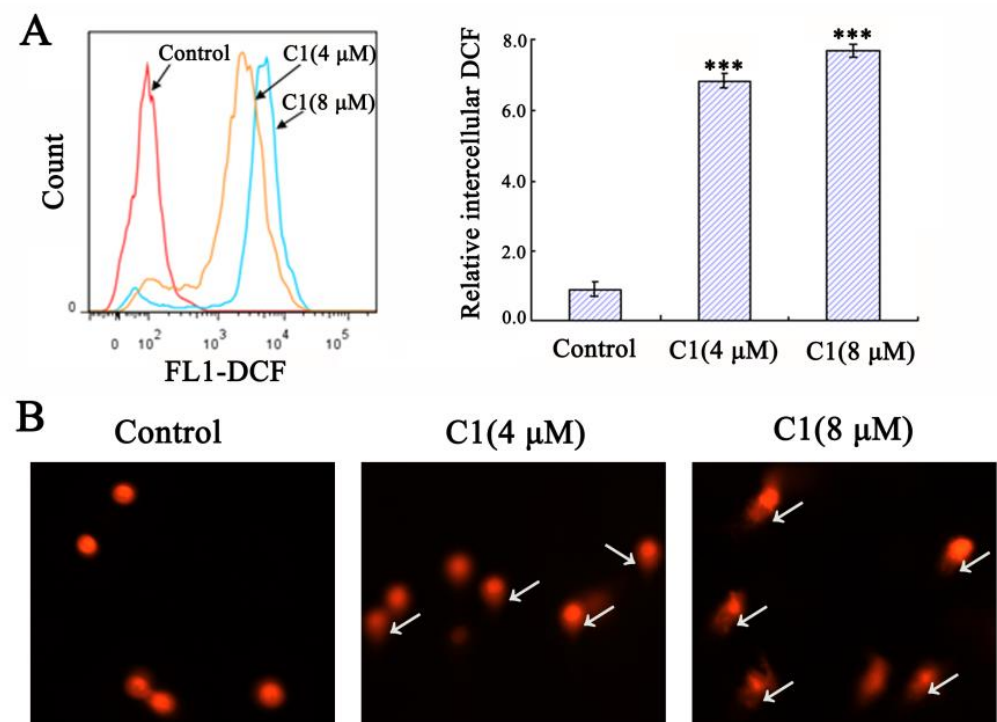


Figure 7. (A) Flow cytometry analysis of ROS level in C1-treated A549 cells. *** $p < 0.001$. (B) DNA fragmentation triggered by C1 in A549 cells, measured using a comet assay (the comet tails marked with white arrows).

Excessive intracellular ROS can cause DNA damage and cell death [43,44]. Next, a comet assay was performed to determine whether C1 caused DNA damage. Undamaged DNA cannot migrate, and fluorescence is only confined to the nucleus. In DNA-damaged cells, negatively charged DNA fragments are then released from the nucleus and migrate towards the anode. There was no comet-like cell observed in the control group. In comparison, C1-treated cells with longer tails (white arrows) were observed, and a higher percentage, indicating the existence of severe DNA fragmentation (Figure 7B). These results strongly suggest that C1 induces DNA damage.

2.6. In Vivo Antitumor Efficacy of C1

Based on these promising biological properties, the in vivo therapeutic efficacy of C1 was further investigated in mice bearing A549 tumors. As displayed in Figure 8A, the tumors grew rapidly in untreated mice. The mice treated with a dose of C1 at 2.5 mg/kg showed slight inhibitory effect on tumor growth, with an inhibition rate of 46.3%. However, the mice injected with a high dose of C1 at 5 mg/kg showed a high therapeutic efficacy (63.5%). Generally, body weight change is considered a key indicator of systemic toxicity. Indeed, no apparent weight loss (Figure 8B) was observed in mice treated with C1 compared to the control group.

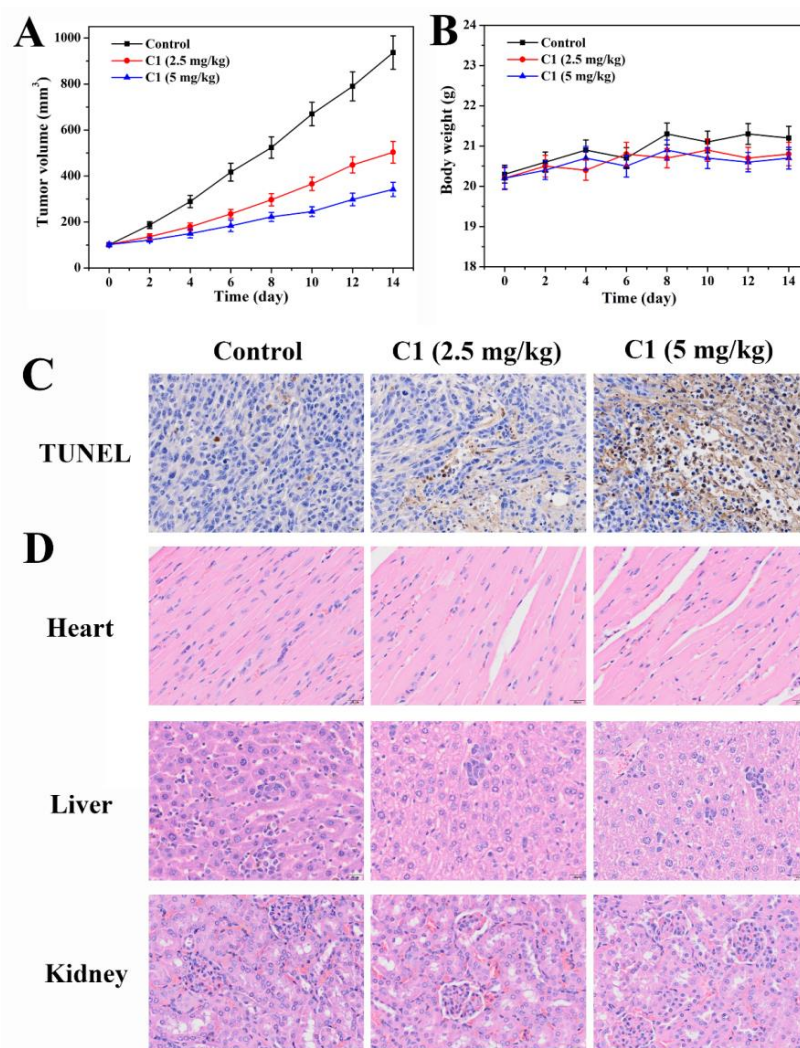


Figure 8. (A) Tumor growth inhibition curves of mice treated with C1. (B) The body weight of the mice throughout the follow-up period in the treatment of C1. (C) TUNEL staining of tumor tissues. (D) H&E staining of the major organs (heart, liver, and kidney).

In addition, TUNEL (terminal deoxynucleotidyl transferase dUTP nick end labeling) staining of tumor tissue sections was performed to examine the effect of C1 on apoptosis *in vivo*. As shown in Figure 8C, the group treated with C1 exhibited notable cell apoptosis, whereas the control group had few apoptotic cells. Histological analyses were carried out using H&E (hematoxylin and eosin) staining to evaluate the toxicity of C1 for the major organ. As shown in Figure 8D, no pathological alterations or other abnormalities were detected in the histological analyses of the heart, liver, and kidney after treatment with C1, indicating that C1 exhibited biocompatibility and biosafety *in vivo*.

3. Materials and Methods

3.1. Reagents and Materials

All chemicals were purchased from InnoChem Company (Beijing, China) or Sigma-Aldrich Company (St. Louis, MO, USA). All cell lines were supplied by the Shanghai Institute for Biochemistry and Cell Biology (Shanghai, China). The cells were cultured at 37 °C in 5% CO₂. Elemental analyses (C, N, and H) were carried out on a Perkin-Elmer 2400 analyzer. Mass spectra of each fragment were measured on a Bruker micrOTOF-Q II. Infrared (IR) spectra were recorded using KBr pellets (4000–400 cm⁻¹) on a Nexus 870 FT-IR spectrophotometer.

3.2. Synthesis of Cu, Zn, and Mn Complexes

The ligands were prepared according to the procedure we reported previously [45]. A mixture of 2-quinolinecarboxaldehyde (3 mmol) and 5-chloro-2-aminophenol (3 mmol) was dissolved in MeOH (20 mL) and heated at 65 °C. After 4 h, the solvent was eliminated under vacuum, then washed with methanol and dried to obtain a yellow powdered ligand.

5-chloro-2-*N*-(2-quinolylmethylene) aminophenol (L). Yield: 89.7%. Elemental analysis for C₁₆H₁₁ClN₂O: C, 67.97; H, 3.92; N, 9.91; O, 5.66. Found: C, 66.79; H, 3.95; N, 9.98; O, 5.74. ¹H NMR (400 MHz, DMSO-*d*₆) δ 9.89 (s, 1H), 8.91 (s, 1H), 8.58–8.47 (m, 2H), 8.13 (d, *J* = 8.4 Hz, 1H), 8.07 (d, *J* = 8.2 Hz, 1H), 7.89–7.80 (m, 1H), 7.74–7.67 (m, 1H), 7.43 (d, *J* = 8.5 Hz, 1H), 7.03 (d, *J* = 2.3 Hz, 1H), 6.94 (d, *J* = 10.8 Hz, 1H). ¹³C NMR (101 MHz, DMSO-*d*₆) δ 160.50, 155.24, 153.02, 147.81, 137.19, 136.30, 132.56, 130.62, 129.67, 128.95, 128.54, 128.35, 121.85, 119.97, 119.23, 116.70. IR spectrum of L1. IR (KBr) peaks: 3736 (ν_{O-H}), 2315, 1796 (ν_{C=N}), 1582, 1500, 1428, 1313, 1223 (ν_{C-N}), 832, 754, and 679 cm⁻¹. ESI-MS: 281.18 [M – H].

Then, 0.1 mmol ligand and 0.1 mmol CuCl₂/ZnCl₂ (containing 1 mL pyridine)/MnCl₂·4H₂O were dissolved in MeOH (20 mL) and refluxed at 65 °C for 4 h. The resulting solution was volatilized naturally at room temperature, and the crystals of Cu, Zn, and Mn complexes were obtained after a week.

5-chloro-2-*N*-(2-quinolylmethylene)aminophenoxide-Cu(II)-chloride(C1). Yield: 73.5%. Solubility in saline: ≥1.9 mg/mL. Melting points: 242 °C. Elemental analysis for C₁₆H₁₀Cl₂CuN₂O: C, 50.48; H, 2.65; N, 7.36; O, 4.20. Found: C, 50.66; H, 2.59; N, 7.31; O, 4.23. IR spectrum of C1. IR (KBr) peaks: 2310, 1795 (ν_{C=N}), 1523, 1243, 1179, 1053 (ν_{C-N}), 843, 749 and 689 cm⁻¹. ESI-MS: 380.00 [M + H]. CCDC No. 1436726.

5-chloro-2-*N*-(2-quinolylmethylene)aminophenoxide-Zn(II)-chloride/pyridine (C2). Yield: 69.8%. Solubility in saline: ≥1.3 mg/mL. Melting points: 217 °C. Elemental analysis for C₂₁H₁₅Cl₂N₃OZn: C, 54.64; H, 3.28; N, 9.10; O, 3.47. Found: C, 54.79; H, 3.25; N, 9.13; O, 3.40. ¹H NMR (400 MHz, DMSO-*d*₆) δ 8.93 (s, 1H), 8.61 (d, *J* = 8.5 Hz, 1H), 8.57–8.52 (m, 2H), 8.26–8.24 (m, 2H), 8.16 (d, *J* = 8.5 Hz, 1H), 8.09 (d, *J* = 7.2 Hz, 1H), 7.89–7.84 (m, 1H), 7.74–7.70 (m, 1H), 7.45 (d, *J* = 8.5 Hz, 1H), 7.29 (d, *J* = 8.5 Hz, 2H), 7.05 (d, *J* = 2.3 Hz, 1H), 6.97–6.94 (m, 1H). ¹³C NMR (101 MHz, DMSO-*d*₆) δ 161.68, 157.86, 156.44, 153.47, 148.30, 144.30, 137.73, 136.70, 132.98, 131.33, 131.15, 129.94, 129.26, 128.74, 128.43, 122.37, 120.47,

119.38, 117.19. IR (KBr) peaks: 2313, 1795 ($\nu_{C=N}$), 1518, 1376, 1251, 1080 (ν_{C-N}), 840, 758, and 641 cm^{-1} . ESI-MS: 458.96 [M]. CCDC No. 2259854.

5-chloro-2-N-(2-quinolylmethylene)aminophenoxide-Mn(II)-chloride/dihydrate (C3). Yield: 64.2%. Solubility in saline: ≥ 0.8 mg/mL. Melting points: 256 °C. Elemental analysis for $\text{C}_{16}\text{H}_{14}\text{Cl}_2\text{MnN}_2\text{O}_3 \cdot \text{CH}_3\text{OH}$: C, 46.39; H, 4.12; N, 6.36; O, 14.54. Found: C, 46.50; H, 4.09; N, 6.31; O, 14.48. IR spectrum of C3. IR (KBr) peaks: 2900 (ν_{H-O-H}), 2314, 1741 ($\nu_{C=N}$), 1583, 1518, 1426, 1235, 1079 (ν_{C-N}), 834, 754, and 690 cm^{-1} . ESI-MS: 335.02 [M-2H₂O-Cl]. CCDC No. 1033296.

3.3. The Stability of Cu, Zn, and Mn Complexes

These metal complexes were dissolved in saline (0.9% sodium chloride solution) and stored at room temperature for 0 h, 24 h, and 48 h, respectively, and their absorbance was determined by UV-vis spectroscopy.

3.4. Wound-Healing Assay

To evaluate the impact of C1 on cell migration, a wound-healing assay was carried out. A549 cells were seeded into 6-well plates and incubated overnight at 37 °C. C1 was dissolved in saline. Subsequently, scratch wounds were performed in the monolayer of cells using sterile toothpicks, and then the cells were treated with the Cu complex (2 μM and 4 μM). The cells were captured using an inverted microscope at 0 and 24 h.

3.5. Transwell Invasion Assay

The effect of C1 on tumor cell invasiveness was assessed by transwell assay. In brief, the transwell chamber was pre-coated with 70 μL diluted matrigel for 8 h at 37 °C. A549 cells were seeded to the upper chamber, and then C1 was added to the chamber. After 24 h of incubation, the chambers were washed, stained with 0.5% crystal violet for 20 min, and captured using an inverted microscope.

3.6. Cell Apoptosis Analysis

The A549 cells were placed in 6-well plates and incubated overnight. The cells were treated with C1 (4 μM and 8 μM) and incubated for 24 h. Subsequently, the cells were harvested and stained with Annexin V/PI for 20 min. The samples were detected by flow cytometry.

3.7. Mitochondrial Membrane Potential ($\Delta\Psi_m$) Assay

Exponentially growing A549 cells were cultured in 6-well plates. Subsequently, C1 (4 μM and 8 μM) was exposed to the cells for 24 h. The cells were stained with JC-1 probe and analyzed by flow cytometry.

3.8. Cell Cycle Analysis

The A549 cells were seeded into 10 cm dishes and incubated overnight. Subsequently, the cells were treated with C1 (4 μM and 8 μM). After 48 h, the cells were collected, fixed with 75% ethanol overnight, stained with PI for 20 min, and measured by flow cytometry.

3.9. β -Galactosidase Staining Assay

A549 cells were cultured in 6-well plates and incubated overnight. After C1 treatment for 24 h, the cells were fixed. Then, 20 min later, the cells were washed and stained with β -galactosidase for 48 h. The stained cells were observed and captured using an inverted microscope.

3.10. Measurement of Cellular ROS

The ROS in A549 cells was analyzed by flow cytometry. After pretreatment with C1 (4 μ M and 8 μ M) for 24 h, the A549 cells were collected and stained with H₂DCF-DA. After 20 min, the samples were measured using a flow cytometer.

3.11. Comet Assay

The A549 cells were seeded into 6-well plates and treated with C1. A mixture of 10 μ L cell suspension and 70 μ L low-melting-point agarose (1%) were placed on a glass microscope slide (pre-coated with 1% normal-melting-point agarose) and covered with coverslips. The cells were separated by gel electrophoresis, stained with PI, and captured using an inverted fluorescence microscope.

3.12. Fluorescence-Quenching Assay

The fluorescence spectrum was performed to measure the interaction mode of C1 (0–16 μ M) and EB-DNA (8 μ M ethidium bromide added into 10 μ M CT-DNA) in a pH 7.2 Tris-HCl buffer. The EB-DNA was excited at 510 nm, and for the emission spectra, the emission range was set to 530–750 nm. C1 was gradually added to the EB-DNA solution.

3.13. Molecular Docking Study

The molecular docking method was performed using AutoDock 4.2. Docking studies were determined using MGL tools with AutoGrid and AutoDock to perform blind docking calculations between both C1 and DNA. The results were analyzed using Pymol software.

3.14. In Vivo Antitumor Experiment

BALB/C nude mice (6–8 weeks old, 18–22 g) were purchased from Hunan SJA Laboratory Animal Co., Ltd. An amount of 200 μ L of A549 cells (containing 2×10^6 cells) were subcutaneously injected into the left flank of the mice. The mice were randomly divided into 3 groups when the average tumor size reached 100 mm³. Then, the mice were treated with saline and C1 (2.5 and 5 mg/kg) for two weeks. C1 was dissolved in saline. During the treatment, the tumor volume and body weight of mice were measured every two days. The major organs (heart, kidney, and liver) and tumor tissues were harvested and sliced for H&E staining and TUNEL staining, respectively.

4. Conclusions

In summary, we designed and synthesized Cu(II), Zn(II), and Mn(II) complexes derived from 5-chloro-2-*N*-(2-quinolylmethylene)aminophenol. Indeed, the Cu complex exhibited effective cytotoxicity toward lung cancer cells and remarkably inhibited A549 cell migration. C1 also displayed an outstanding inhibitory effect against A549 tumor growth in vivo. Furthermore, we confirmed the mechanism of tumor growth inhibition by inducing mitochondrial apoptosis, interacting with DNA, blocking cell cycle arrest, inducing cell senescence, and inducing DNA damage.

Supplementary Materials: The following supporting information can be downloaded at: <https://www.mdpi.com/article/10.3390/molecules28124876/s1>, Figures S1–S12: The IR, NMR, and ESI-MS of ligand and complexes; Figure S13: UV-vis spectra of complexes C1–C3. Table S1: Crystal data and structure refinement for C1–C3; Table S2: Bond lengths/Å and bond angles/° for C1–C3. The complete crystallography data of C1–C3 can be obtained free of charge from the Cambridge Crystallographic Data Centre via www.ccdc.cam.ac.uk/structures, accessed on 30 May 2023, with CCDC numbers of 1436726 (for C1), 2259854 (for C2), and 1033296 (for C3).

Author Contributions: Conceptualization, M.J.; methodology, S.G.; software, L.H. and S.G.; validation, L.H., M.H. and S.G.; formal analysis, S.G.; investigation, L.H., M.H. and S.G.; resources, M.J.; data curation, X.Z.; writing—original draft preparation, S.G.; writing—review and editing, M.J.; visualization, X.Z.; supervision, C.J.; project administration, Y.Q. and M.J.; funding acquisition, Y.Q. and M.J. All authors have read and agreed to the published version of the manuscript.

Funding: This work was supported by the Natural Science Foundation of China (22077021), the Natural Science Foundation of Guangxi (2022GXNSFGA035003), the Natural Science Foundation of Guangxi Science and Technology Normal University (GXKS2023ZDA001, GXKS2023ZDA003), and the “Research on the Substance Basis and Mechanism of Action of Zhuang and Yao Medicine” Innovation Team.

Institutional Review Board Statement: All animal experiments complied with the regulations from the People’s Republic of China’s Ministry of Health (document nos. 55, 2001) Committee’s Care and Use of Animals. The mice were supplied by Hunan SJA Laboratory Animal Co., Ltd. China (Certificate No. SCXK2019-0004).

Data Availability Statement: Data will be made available upon request.

Conflicts of Interest: The authors declare no conflict of interest.

Sample Availability: Samples of the compounds (C1–C3) are available from the authors.

References

1. Ghosh, S. Cisplatin: The first metal based anticancer drug. *Bioorg. Chem.* **2019**, *88*, 102925. [[CrossRef](#)] [[PubMed](#)]
2. Du, J.; Wang, X.; Li, Y.; Ren, X.; Zhou, Y.; Hu, W.; Zhou, C.; Jing, Q.; Yang, C.; Wang, L. DHA exhibits synergistic therapeutic efficacy with cisplatin to induce ferroptosis in pancreatic ductal adenocarcinoma via modulation of iron metabolism. *Cell Death Dis.* **2021**, *12*, 705. [[CrossRef](#)] [[PubMed](#)]
3. Galluzzi, L.; Vitale, I.; Michels, J.; Brenner, C.; Szabadkai, G.; Harel-Bellan, A.; Castedo, M.; Kroemer, G. Systems biology of cisplatin resistance: Past, present and future. *Cell Death Dis.* **2014**, *5*, e1257. [[CrossRef](#)] [[PubMed](#)]
4. Galluzzi, L.; Senovilla, L.; Vitale, I.; Michels, J.; Martins, I.; Kepp, O.; Castedo, M.; Kroemer, G. Molecular mechanisms of cisplatin resistance. *Oncogene* **2012**, *31*, 1869–1883. [[CrossRef](#)] [[PubMed](#)]
5. Romani, A.M. Cisplatin in cancer treatment. *Biochem. Pharmacol.* **2022**, *206*, 115323. [[CrossRef](#)]
6. Callejo, A.; Sedó-Cabezón, L.; Domenech Juan, I.; Llorens, J. Cisplatin-induced ototoxicity: Effects, mechanisms and protection strategies. *Toxics* **2015**, *3*, 268–293. [[CrossRef](#)]
7. Sancho-Garnier, H.; Colonna, M. Breast cancer epidemiology. *Presse Med.* **2019**, *48*, 1076–1084. [[CrossRef](#)]
8. Li, N.; Deng, Y.; Zhou, L.; Tian, T.; Yang, S.; Wu, Y.; Zheng, Y.; Zhai, Z.; Hao, Q.; Song, D. Global burden of breast cancer and attributable risk factors in 195 countries and territories, from 1990 to 2017: Results from the Global Burden of Disease Study 2017. *J. Hematol. Oncol.* **2019**, *12*, 140. [[CrossRef](#)]
9. Dai, Y.; Zhu, Y.; Cheng, J.; Shen, J.; Huang, H.; Liu, M.; Chen, Z.; Liu, Y. Nitric oxide-releasing platinum (IV) prodrug efficiently inhibits proliferation and metastasis of cancer cells. *Chem. Commun.* **2020**, *56*, 14051–14054. [[CrossRef](#)]
10. Ayipo, Y.O.; Osunniran, W.A.; Mordi, M.N. Metal complexes of β -carboline: Advances in anticancer therapeutics. *Coord. Chem. Rev.* **2021**, *432*, 213746. [[CrossRef](#)]
11. Gourdon, L.; Cariou, K.; Gasser, G. Phototherapeutic anticancer strategies with first-row transition metal complexes: A critical review. *Chem. Soc. Rev.* **2022**, *51*, 1167–1195. [[CrossRef](#)] [[PubMed](#)]
12. Heras, B.L.; Amesty, Á.; Estévez-Braun, A.; Hortelano, S. Metal complexes of natural product like-compounds with antitumor activity. *Anti-Cancer Agents Med. Chem.* **2019**, *19*, 48–65. [[CrossRef](#)] [[PubMed](#)]
13. Gou, Y.; Huang, G.; Li, J.; Yang, F.; Liang, H. Versatile delivery systems for non-platinum metal-based anticancer therapeutic agents. *Coord. Chem. Rev.* **2021**, *441*, 213975. [[CrossRef](#)]
14. Paprocka, R.; Wiese-Szadkowska, M.; Janciauskiene, S.; Kosmalski, T.; Kulik, M.; Helmin-Basa, A. Latest developments in metal complexes as anticancer agents. *Coord. Chem. Rev.* **2022**, *452*, 214307. [[CrossRef](#)]
15. Silva, C.S.; Moutinho, C.; Ferreira da Vinha, A.; Matos, C. Trace minerals in human health: Iron, zinc, copper, manganese and fluorine. *Int. J. Sci. Res. Methodol.* **2019**, *13*, 57–80.
16. Zabłocka-Słowińska, K.; Płaczkowska, S.; Prescha, A.; Pawełczyk, K.; Porębska, I.; Kosacka, M.; Pawlik-Sobecka, L.; Grajeta, H. Serum and whole blood Zn, Cu and Mn profiles and their relation to redox status in lung cancer patients. *J. Trace Elem. Med. Biol.* **2018**, *45*, 78–84. [[CrossRef](#)]
17. Bocca, B.; Ruggieri, F.; Pino, A.; Rovira, J.; Calamandrei, G.; Martínez, M.Á.; Domingo, J.L.; Alimonti, A.; Schuhmacher, M. Human biomonitoring to evaluate exposure to toxic and essential trace elements during pregnancy. Part A. concentrations in maternal blood, urine and cord blood. *Environ. Res.* **2019**, *177*, 108599. [[CrossRef](#)]
18. Pellei, M.; Del Bello, F.; Porchia, M.; Santini, C. Zinc coordination complexes as anticancer agents. *Coord. Chem. Rev.* **2021**, *445*, 214088. [[CrossRef](#)]
19. Kovala-Demertzi, D.; Staninska, M.; Garcia-Santos, I.; Castineiras, A.; Demertzis, M.A. Synthesis, crystal structures and spectroscopy of meclofenamic acid and its metal complexes with manganese (II), copper (II), zinc (II) and cadmium (II). Antiproliferative and superoxide dismutase activity. *J. Inorg. Biochem.* **2011**, *105*, 1187–1195. [[CrossRef](#)]
20. Parekh, N.M.; Mistry, B.M.; Pandurangan, M.; Shinde, S.K.; Patel, R.V. Investigation of anticancer potencies of newly generated Schiff base imidazolylphenylheterocyclic-2-ylmethylenethiazole-2-amines. *Chin. Chem. Lett.* **2017**, *28*, 602–606. [[CrossRef](#)]

21. Hameed, A.; Al-Rashida, M.; Uroos, M.; Abid Ali, S.; Khan, K.M. Schiff bases in medicinal chemistry: A patent review (2010–2015). *Expert Opin. Ther. Pat.* **2017**, *27*, 63–79. [[CrossRef](#)] [[PubMed](#)]
22. Alam, A.; Ali, M.; Latif, A.; Rehman, N.U.; Saher, S.; Khan, A.; Ullah, S.; Ullah, O.; Halim, S.A.; Sani, F. Novel Bis-Schiff's base derivatives of 4-nitroacetophenone as potent α -glucosidase agents: Design, synthesis and in silico approach. *Bioorg. Chem.* **2022**, *128*, 106058. [[CrossRef](#)] [[PubMed](#)]
23. Agbektas, T.; Zontul, C.; Ozturk, A.; Huseynzada, A.; Ganbarova, R.; Hasanova, U.; Cinar, G.; Tas, A.; Kaya, S.; Chtita, S. Effect of azomethine group containing compounds on gene profiles in Wnt and MAPK signal patterns in lung cancer cell line: In Silico and In Vitro analyses. *J. Mol. Struct.* **2023**, *1275*, 134619. [[CrossRef](#)]
24. Tan, Y.-X.; Zhang, Z.-J.; Liu, Y.; Yu, J.-X.; Zhu, X.-M.; Kuang, D.-Z.; Jiang, W.-J. Synthesis, crystal structure and biological activity of the Schiff base organotin(IV) complexes based on salicylaldehyde-o-aminophenol. *J. Mol. Struct.* **2017**, *1149*, 874–881. [[CrossRef](#)]
25. Wazalwar, S.S.; Banpurkar, A.R.; Perdihi, F. Synthesis, Characterization, Molecular Docking Studies and Anticancer Activity of Schiff Bases Derived from 3-(Substituted phenyl)-1-phenyl-1H-pyrazole-4-carbaldehyde and 2-Aminophenol. *J. Chem. Crystallogr.* **2018**, *48*, 185–199. [[CrossRef](#)]
26. Liu, X.; Hamon, J.-R. Recent developments in penta-, hexa- and heptadentate Schiff base ligands and their metal complexes. *Coord. Chem. Rev.* **2019**, *389*, 94–118. [[CrossRef](#)]
27. Alfonso-Herrera, L.A.; Rosete-Luna, S.; Hernández-Romero, D.; Rivera-Villanueva, J.M.; Olivares-Romero, J.L.; Cruz-Navarro, J.A.; Soto-Contreras, A.; Arenaza-Corona, A.; Morales-Morales, D.; Colorado-Peralta, R. Transition Metal Complexes with Tridentate Schiff Bases (O N O and O N N) Derived from Salicylaldehyde: An Analysis of Their Potential Anticancer Activity. *Chemmedchem* **2022**, *17*, e202200367. [[CrossRef](#)] [[PubMed](#)]
28. Jana, N.C.; Patra, M.; Brandão, P.; Panja, A. Synthesis, structure and diverse coordination chemistry of cobalt (III) complexes derived from a Schiff base ligand and their biomimetic catalytic oxidation of o-aminophenols. *Polyhedron* **2019**, *164*, 23–34. [[CrossRef](#)]
29. Panja, A.; Shyamal, M.; Saha, A.; Mandal, T.K. Methylene bridge regulated geometrical preferences of ligands in cobalt (III) coordination chemistry and phenoxazinone synthase mimicking activity. *Dalton Trans.* **2014**, *43*, 5443–5452. [[CrossRef](#)]
30. Abd El-Halim, H.F.; Mohamed, G.G.; Anwar, M.N. Antimicrobial and anticancer activities of Schiff base ligand and its transition metal mixed ligand complexes with heterocyclic base. *Appl. Organomet. Chem.* **2018**, *32*, e3899. [[CrossRef](#)]
31. Gurgul, I.; Janczy-Cempa, E.; Mazuryk, O.; Lekka, M.; Łomzik, M.; Suzenet, F.; Gros, P.C.; Brindell, M. Inhibition of Metastasis by Polypyridyl Ru (II) Complexes through Modification of Cancer Cell Adhesion—In Vitro Functional and Molecular Studies. *J. Med. Chem.* **2022**, *65*, 10459–10470. [[CrossRef](#)] [[PubMed](#)]
32. Zhang, Q.; Liu, F.; Chen, W.; Miao, H.; Liang, H.; Liao, Z.; Zhang, Z.; Zhang, B. The role of RNA m5C modification in cancer metastasis. *Int. J. Biol. Sci.* **2021**, *17*, 3369. [[CrossRef](#)]
33. Duff, D.; Long, A. Roles for RACK1 in cancer cell migration and invasion. *Cell Signal.* **2017**, *35*, 250–255. [[CrossRef](#)] [[PubMed](#)]
34. Lyden, D.; Ghajar, C.M.; Correia, A.L.; Aguirre-Ghiso, J.A.; Cai, S.; Rescigno, M.; Zhang, P.; Hu, G.; Fendt, S.-M.; Boire, A. Metastasis. *Cancer Cell* **2022**, *40*, 787–791. [[CrossRef](#)] [[PubMed](#)]
35. Brindell, M.; Gurgul, I.; Janczy-Cempa, E.; Gajda-Morszewski, P.; Mazuryk, O. Moving Ru polypyridyl complexes beyond cytotoxic activity towards metastasis inhibition. *J. Inorg. Biochem.* **2022**, *226*, 111652. [[CrossRef](#)] [[PubMed](#)]
36. Al-Aamri, H.M.; Irving, H.R.; Bradley, C.; Meehan-Andrews, T. Intrinsic and extrinsic apoptosis responses in leukaemia cells following daunorubicin treatment. *BMC Cancer* **2021**, *21*, 438. [[CrossRef](#)] [[PubMed](#)]
37. Huang, K.B.; Wang, F.Y.; Tang, X.M.; Feng, H.W.; Chen, Z.F.; Liu, Y.C.; Liu, Y.N.; Liang, H. Organometallic gold (III) complexes similar to tetrahydroisoquinoline induce ER-stress-mediated apoptosis and pro-death autophagy in A549 cancer cells. *J. Med. Chem.* **2018**, *61*, 3478–3490. [[CrossRef](#)]
38. Das, A.; Mohammed, T.P.; Kumar, R.; Bhunia, S.; Sankaralingam, M. Carbazole appended trans-dicationic pyridinium porphyrin finds supremacy in DNA binding/ photocleavage over a non-carbazolyl analogue. *Dalton Trans.* **2022**, *51*, 12453–12466. [[CrossRef](#)]
39. Rafique, B.; Kalsoom, S.; Sajini, A.A.; Ismail, H.; Iqbal, M. Synthesis, Characterization, Biological Evaluation and DNA Interaction Studies of 4-Aminophenol Derivatives: Theoretical and Experimental Approach. *Molecules* **2022**, *27*, 1352. [[CrossRef](#)]
40. Gałczyńska, K.; Drulis-Kawa, Z.; Arabski, M. Antitumor activity of Pt (II), Ru (III) and Cu (II) complexes. *Molecules* **2020**, *25*, 3492. [[CrossRef](#)]
41. Park, C.W.; Bak, Y.; Kim, M.J.; Srinivasrao, G.; Hwang, J.; Sung, N.K.; Kim, B.Y.; Yu, J.-H.; Hong, J.T.; Yoon, D.-Y. The Novel Small Molecule STK899704 Promotes Senescence of the Human A549 NSCLC Cells by Inducing DNA Damage Responses and Cell Cycle Arrest. *Front. Pharmacol.* **2018**, *9*, 163. [[CrossRef](#)] [[PubMed](#)]
42. Simon, H.U.; Haj-Yehia, A.; Levi-Schaffer, F. Role of reactive oxygen species (ROS) in apoptosis induction. *Apoptosis* **2000**, *5*, 415–418. [[CrossRef](#)] [[PubMed](#)]
43. Srinivas, U.S.; Tan, B.W.Q.; Vellayappan, B.A.; Jeyasekharan, A.D. ROS and the DNA damage response in cancer. *Redox Biol.* **2018**, *25*, 101084. [[CrossRef](#)] [[PubMed](#)]

44. Zhang, Y.J.; Yang, D.L.; Qin, H.X.; He, L.J.; Huang, J.H.; Tang, D.Y.; Xu, Z.G.; Chen, Z.Z.; Li, Y. DMAPT-D6 induces death-receptor-mediated apoptosis to inhibit glioblastoma cell oncogenesis via induction of DNA damage through accumulation of intracellular ROS. *Oncol. Rep.* **2021**, *45*, 1261–1272. [[CrossRef](#)]
45. Gai, S.S.; Jiang, M. Biological properties of Cu(II) complex with human serum albumin. *Huaxue Tongbao* **2018**, *81*, 253–257.

Disclaimer/Publisher's Note: The statements, opinions and data contained in all publications are solely those of the individual author(s) and contributor(s) and not of MDPI and/or the editor(s). MDPI and/or the editor(s) disclaim responsibility for any injury to people or property resulting from any ideas, methods, instructions or products referred to in the content.